Selective Formation and Removal of Liquid Microlenses at Predetermined Locations Within Microfluidics Through Pneumatic Control

Liang Dong, *Member, IEEE*, and Hongrui Jiang, *Member, IEEE*

***Abstract*—This paper reports on liquid (deionized water) microlenses that are intrinsically formed and integrated within microfluidics through pneumatic manipulation of fluids inside microchannels. Such microlenses are formed via liquid–air interfaces of liquid droplets, which are pinned at T-shaped junctions of channels. In addition to being tunable in focal lengths (a few hundreds of micrometers to ∞) along the microchannels parallel to the substrate used, these microlenses can uniquely be repositioned, removed, and reformed at predetermined locations of the T-shaped junctions within microchannels on demand under pneumatic controls. The design and formation of a microfluidic channel network for the *in situ* formation are first described. Then, the pneumatic control of the fluids, including the formation, movement, and size control of a lens droplet, is discussed, and the *in situ* formation processes for single and multiple liquid microlenses are described. The *in situ* formation processes for a single microlens and a two-lens combination only take tens of seconds, eliminating various conventional microfabrication processes and multiple layers of materials. Finally, the detail of characterization of these microlenses is given. [2007-0176]**

***Index Terms*—Liquid microlens, microfluidics, optofluidics, pneumatic control, tunable.**

I. Introduction

LENSES are important optical components. With continuing miniaturization trends across various fields, microlenses have been developed and have found applications in many fields such as medical diagnostics [1]–[3], optical communication [4], optical storage [5], biomimetic optics [6], [7], biosensing [8], biochemical analysis [9], [10], biomedical diagnosis [11], and lab-on-a-chip systems [12]–[17]. Diverse microfabrication processes have been employed to realize microlenses, including photoresist reflow [18], [19], isotropic etching of silica glass and silicon [20], [21], inkjet printing [22], [23], modified LIGA process [24], [25], and self-assembly process [26], [27]. However, these microlenses are generally fixed in their shapes; thus, they are nontunable in focal lengths. Many optical systems require the focal lengths to be tunable. Traditional approach to realizing the focal-length tuning is to displace the fixed focal lenses involved [28], requiring complicated mechanical components (e.g., gears, motors, and rails). Although it is straightforward to realize tunable micro-optics by miniaturizing and assembling these discrete components, this approach is complicated considering the diversity in the fabrication process for each component, thus remaining challenging so far. Therefore, tunable-microlens technology is appealing and has attracted considerable research efforts [29].

Emerging tunable microlenses have exhibited the potential to miniaturize and advance optical systems without the need for the mechanical parts. They can distinctly benefit the implementation of compact and low-cost optical systems, impacting significantly on a multitude of fields [29]. Generally, microlens tuning is realized by either changing the shape of the lens or changing the refractive indexes of the materials involved. A variety of tunable liquid-microlens technologies have been demonstrated to simplify lens tuning, including reorientation of liquid crystal [30], [31], electrowetting [32], [33] electrochemical activation of liquid droplet [34], mechanical actuation of polymeric material [35], [36], and self-adaptation to environmental parameters using responsive polymers [37]–[40]. Despite these progresses in focal-length tuning, these tunable microlenses, in general, not only rely on costly microfabrication processes and various functional materials but also have little flexibility—their positions are fixed once produced at the designated locations, and they are difficult to be removed and reformed on demand. This limits the degree of tunability and reconfigurability in many cases. Moreover, these lenses usually have their optical axes perpendicular to the substrates such that other optical components involved (e.g., light source and photodetector) have to be laid out in different layers. It gives rise to the complexity in the integration of these components since multiple-layer structures, time-consuming optical alignment between multiple layers, and stringent optical designs for ray tracing within a microsystem are needed.

We are interested in taking advantages of the microfluidic technology to realize liquid (here, deionized water) microlenses through *in situ* formation within microfluidic channels, aiming to implement not only tuning in focal lengths but also repositioning, removal, and reformation of the lenses upon request

Manuscript received July 16, 2007; revised October 22, 2007. This work was supported in part by the U.S. Department of Homeland Security under Grant N-00014-04-1-0659 awarded to the National Center for Food Protection and Defense at the University of Minnesota and in part by the U.S. National Science Foundation (under Grant ECCS 0622202). Subject Editor O. Solgaard.

L. Dong was with the Department of Electrical and Computer Engineering, University of Wisconsin, Madison, WI 53706 USA. He is now with the Department of Electrical and Computer Engineering, Iowa State University, Ames, IA 50011 USA.

H. Jiang is with the Department of Electrical and Computer Engineering, University of Wisconsin, Madison, WI 53706 USA (e-mail: hongrui@engr.wisc.edu).

Color versions of one or more of the figures in this paper are available online at http://ieeexplore.ieee.org.

Digital Object Identifier 10.1109/JMEMS.2007.912702

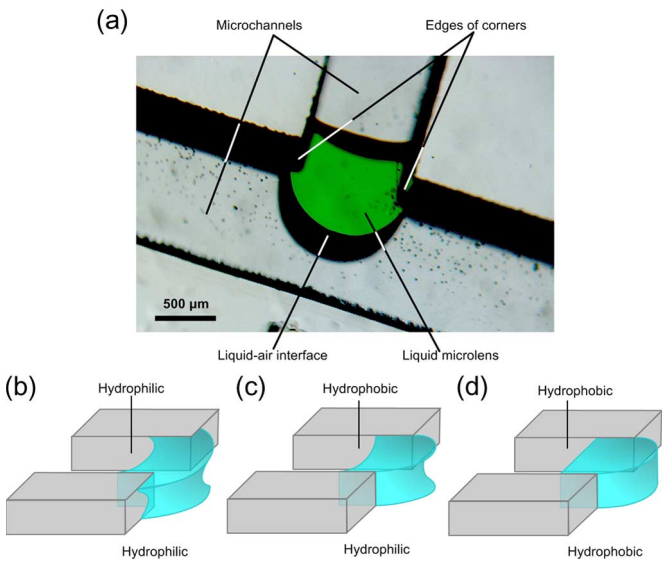

Fig. 1. (a) Optical image of an *in situ*-formed liquid microlens pinned at a T-shaped junction of two channels. The liquid–air interfaces of the lens droplet are perpendicular to the top and bottom glass substrates. (b) Schematic of a water droplet when all the inner surfaces of a channel are hydrophilic. (c) Schematic of a water droplet when the top and bottom substrates of a channel are hydrophilic and its sidewalls are hydrophobic. (d) Schematic of a water droplet when all the inner surfaces of a channel are hydrophobic (water contact angles: 90°).

under pneumatic controls. In addition, the liquid microlenses with optical axes parallel to the substrate used can provide more configuration possibilities, not limited to the ones vertical to the substrates, thus giving more flexibility in designing reconfigurable microoptics within microfluidics. We recently reported the preliminary results on the realization of *in situ*-formed liquid microlenses in microfluidic channels and their application to enhancing fluorescence detection in microfluidics [41], [42]. In this paper, we describe in detail the formation and characterization of these liquid microlenses that are intrinsically integrated within microfluidics by leveraging microfluidic technology, surface chemistry, and pneumatic control.

II. Principle and Structures

The liquid microlens that are *in situ*-formed within microfluidics is shown in Fig. 1(a). By taking advantages of the liquid-surface tension at the microscale, the microlens is formed via the liquid–air interfaces of a liquid (deionized water) droplet generated at a T-shaped junction of microfluidic channels. Since surface tension at the microscale plays a dominant role in liquid behavior over gravity [43], it can maintain robust liquid microlenses. Here, we use pneumatic method to perform the fluid manipulation. Briefly, to form a lens droplet, a liquid droplet is pneumatically chopped from a static fluid and is then guided along the designated channels to a desired junction under air pressures applied. Note that the contact angle of the liquid droplet in a channel has a significant effect on the shape of the liquid droplet. For example, concave menisci occur at the two liquid–air interfaces of a water droplet when all the inner surfaces of a channel are hydrophilic (e.g., untreated glass), and this droplet can go over the corners of a junction even under a low-pressure drop across the droplet [Fig. 1(b)]. In the case where the top and bottom substrates of a channel are hydrophilic (e.g., untreated glass) and its sidewalls are hydrophobic [e.g., polydimethylsiloxane (PDMS)], the water droplet bears a shape of a saddle—convex when looking from the top, whereas concave when looking from the side—since the movement of a water droplet is restricted only along the sidewalls [Fig. 1(c)]. Therefore, the inner surfaces of the channels are chemically treated to form a hydrophobic monolayer onto them so that the liquid–air interfaces of the droplet become perpendicular to both the top and bottom surfaces, and the interface in contact with the edges of the corners is restricted in movement due to high surface energy presented at the corners [Fig. 1(d)].

When an air-pressure difference applied to the droplet equals the internal capillary pressure caused by the curvature difference between the liquid–air interfaces of the droplet, the liquid–air interface at the junction can protrude out of the channel and be steadily pinned along the edges; the shape of the other liquid–air interface, on the other hand, depends on the static contact angle of the liquid on the channel material under homogeneous pneumatic pressure [42]. Thus, a cylindrical liquid microlens is formed with the optical axis in plane with the substrate.

Because of the pinning effect, the shape of the pinned liquid–air interface is flexibly adjustable by changing the air-pressure difference within a certain range. This causes a change in the focal length of the microlens. Aside from focal-length tuning, the microlens can be further reconfigured with high flexibility within the channel network due to the fluidic nature of the liquid; the repositioning, relocation, removal, and reformation of the microlens under various pressure drops across it will be discussed later.

III. Microfluidic Setup

A. Microfluidic Setup

A typical microfluidic setup for *in situ* formation of liquid microlenses is schematically shown in Fig. 2. It includes a microfluidic channel network, a fluid delivery control, two pneumatic pressure controls for handling fluids, and multiple connections for access to the channel network.

In the microfluidic channel network, a main channel connects to syringe fluid pump F1 (Harvard Apparatus PHD 2000 Programmable) at a fluidic inlet. A lens channel (1.8 mm in length) is positioned perpendicular to the main channel at junction J2 (5 mm distant to J1). To realize multiple liquid microlenses, a small step is produced in the middle along the length of the lens channel by reducing its width to form junction J3, the surface of which being vertical to the sidewalls of the channel. Air channel AC1 is branched from the main channel at junction J1 (15 mm away from the fluidic inlet), and air channel AC2 parallel to the main channel is coupled to the lens channel at junction J4. These two air channels allow for applying air pressures to pneumatically control the behavior of a fluid within the channels. Each channel is 450 μm deep and 1 mm wide, except that the part of the lens channel from J3 to J4 is 750 μm

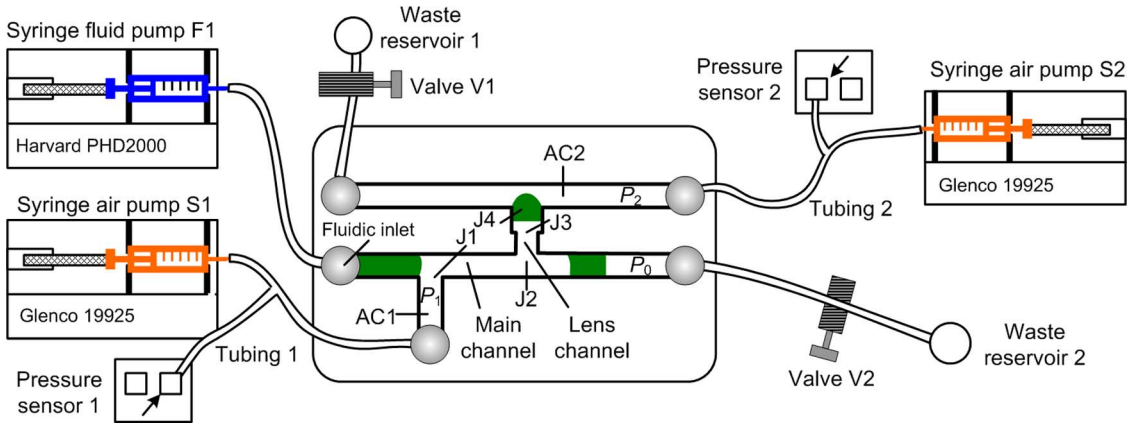

Fig. 2. Schematic of a microfluidic setup for *in situ* formation of a liquid microlens. The width of all microchannels is 1 mm except between junctions J2 and J3 which is 0.75 mm.

wide. This channel network is made between two glass slides, and the cross section of these channels is rectangular.

To deliver liquid (lens material) to the channel network, syringe fluid pump F1 is coupled to the main channel at a fluidic inlet. The air pressures P_1 and P_2 in AC1 and AC2 are adjusted by air-pressure controls S1 and S2, respectively, for manipulating the fluid. Each pressure control consists of a programmable syringe air pump (Spectrum Chromatography, Glenco 19925 series, Houston, TX) and a pressure sensor [Honeywell (model 142PC30D), Morristown, NJ]. The pressure range and the sensitivity of this pressure sensor are 0–30 $\mathrm{lbf/in^2}$ and 166.7 $\mathrm{mV/lbf/in^2}$, respectively. These syringes are connected to PDMS connectors adhered to the channels by silicone tubings. One waste reservoir located outside the device connects to air channel AC2 through valve V1, and another waste reservoir connects to the main channel through another valve V2.

B. Fabrication of Microfluidic Channels

1) Materials: The microchannel network is fabricated through liquid-phase photopolymerization of photosensitive polymers without the need for a cleanroom [44]. Photolithographic procedure is carried out using a desktop EXFO A400 (Mississauga, Ontario, Canada) ultraviolet (UV) light source. High-resolution (3600 dpi) film photomask (Silverline Studio, Madison, WI) is used to transfer patterns to the photosensitive polymer. Here, the photosensitive prepolymer solution [isobornyl acrylate (IBA)] used for channel material, similar to negative photoresist, consists of three constituents in the following ratios: $31.66:1.66:1.0 \rightarrow$ monomer—IBA, cross-linker—tetraethylene glycol dimethacrylate (Sigma–Aldrich, Inc., St. Louis, MO), and photoinitiator—2,2-dimethoxy-2-phenylacetophenone (Sigma–Aldrich, Inc., St. Louis, MO). Exposure to a UV light source causes the prepolymer solution to harden [called poly(IBA)].

2) Formation of Channel Network: As shown in Fig. 3, a cavity is created between two glass slides with 470-μm-thick double-sided adhesive tape (3M, St. Paul, MN). The filling holes (these holes are used as the entrances to fill the liquid-based prepolymer into the cavity), as well as the inlets and

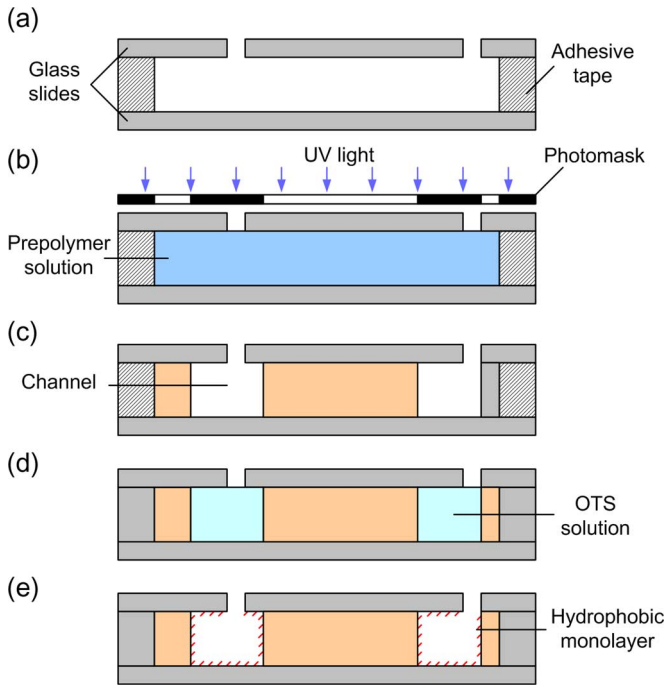

Fig. 3. Fabrication process of microfluidic channels using liquid-phase photopolymerization based on UV photolithography with a single photomask film.

outlets of the device (2 mm in diameter), were previously punched on the top glass slide using a mechanical driller. To improve the adhesion between the adhesive tape and the glass, the device is put on a hot plate at 50 °C for 5 min. Then, the IBA-based prepolymer is flowed into the cavity using a transfer pipette through a filling hole. After that, the microchannels are patterned inside the cavity using a single photomask film. The UV light intensity and exposure time are 7.8 $\mathrm{mW/cm^2}$ and 24 s, respectively. The photomask is then removed, and the device is developed in a bath of ethanol (200 proof) for 100 s. Next, a peristaltic pump is used to flush away the unpolymerized precursor, leaving behind a hardened poly(IBA) microchannel network. The polymer channel definition step, from start to finish, takes about 3 min. Finally, the device is softbaked on a hot plate at 50 °C for 10 min.

3) Surface-Chemistry Treatment: For the purpose of surface-chemistry treatment, an octadecyltrichlorosilane (OTS)

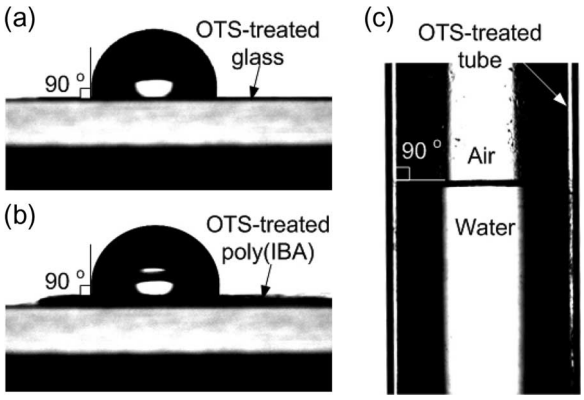

Fig. 4. Surface-chemistry treatment. (a) and (b) Optical images of two water droplets on planar poly(IBA) (top) and glass substrates (bottom) treated with an OTS solution. (c) Optical image of a water–air interface within a glass tube treated with the same OTS solution as in (a) and (b).

solution diluted by hexadecane [0.15% (v/v)] is flowed into the microchannels using a transfer pipette through a filling hole. The solution is maintained for 3 min. After that, the microchannels are cleaned by subsequently flushing 20 ml of methanol, which is followed by drying with a stream of nitrogen. Thus, a self-assembly monomer hydrophobic layer is formed.

The static water contact angle is measured on planar substrates, i.e., a poly(IBA) plate and a glass slide. Both substrates are rinsed in the same OTS solution with that for the microchannels for 3 min. Using a goniometer (OCA 5, DataPhysics Instruments GmbH, Filderstadt, Germany), it is found that the water contact angles on both substrates are $90^\circ \pm 1.8^\circ$, as shown in Fig. 4(a) and (b). Also, we load a water droplet into a glass tube (inner diameter: 1 mm) treated with the same OTS solution. The water–air interface in the tube turns out to be perpendicular to the sidewall, as shown in Fig. 4(c). This means that, through the surface chemistry treatment, both liquid–air interfaces of a water droplet in the microchannels can be perpendicular to the top and bottom glass substrates. Since the surface energy at the poly(IBA) sidewalls of the microchannels is increased, the edges of the corners in the microchannels form geometric barriers to the displacement of the microlens droplet; otherwise, the water droplet would easily get over these corners from one microchannel to another.

C. Access to Microfluidic Setup

Connectors are fabricated to provide access to the device and microchannels. In short, PDMS slabs are constructed with an adhesive layer on the bottom to adhere to the inlets and outlets on the top glass substrate. Details can be found in [45]. Microline tubing (inner diameter: 0.51 mm and outer diameter: 1.52 mm; Cole-Parmer Instrument Company, Vernon Hills, IL) is routed inside the cored PDMS connector and permits delivery of liquids used.

IV. Pneumatic Control of Microfluidics

The *in situ* formation of liquid microlenses involves multiple pneumatic controls of fluids within microchannels, including cutting a droplet out of a static flow and controlling the size of a lens droplet; the reconfiguration of liquid microlenses depends on a threshold pressure drop across the lens droplet. We have experimentally investigated these individual microfluidic operations, thus giving guidance to the formation of the microlenses and the control of their behaviors. We use deionized water to form microlenses. Other liquids could also be potential candidates for lens material, if they possess a high surface tension that allows for a shape of a lens, and can be driven to flow and be controlled within microchannels. For easier visualization, a green food dye is added into the lens liquid (deionized water) for better visualization.

A. Generating a Droplet

A liquid droplet is formed by cutting a static flow at a junction of channels. As shown in Fig. 5(a), a flow enters into a branch channel when passing through junction J1 and then stops flowing. An air pressure is applied to break down the static fluid from the branch channel (air conduit), thus producing a liquid droplet. Considering the relatively poor controllability of the droplet under pneumatic drive, we choose a low air pressure for a slow movement of the droplet along the channel. Therefore, we measure the minimum air pressure at which a liquid droplet can be cut off from the static fluid. In this paper, we gradually increase P_1 from $P_0 + 15$ Pa to $P_0 + 350$ Pa in steps of 10 Pa by injecting air into air conduit AC1 (the other side of the fluid is kept at atmospheric pressure P_0). The injection rate is kept to be 4.7 $\mu\mathrm{L}/\min$ for each injection. For a 1-mm-wide and 450-μm-deep channel, the minimum P_1 of $P_0 + 285$ Pa is found to form a droplet of 0.75 μL at the junction and to move the droplet along a straight channel.

B. Controlling the Size of a Lens Droplet

By combining the use of air pressures P_1 and P_2 from air controls S1 and S2, the size of the lens droplet can be pneumatically controlled. As shown in Fig. 5(b), when passing a T-shaped junction under P_1, a water droplet segmented by air is split into two parts—one (desired lens droplet) going into the lens channel, and the other going in the original direction toward the external environment (atmospheric pressure) through an outlet. The pressure at the other side of the lens droplet is P_2. The volumes of these two parts depend on the pressure difference across each part, i.e., $P_1 - P_0$ and $P_1 - P_2$. When $P_2 = P_0$, the lens droplet (V_{lens}) has the same volume as the other droplet (V_{other}). When $P_2 > P_0$, V_{lens} is less than V_{other}; as P_2 is increased up to a critical value, the entire water droplet tends to flow through the junction into the right side. On the other hand, when $P_2 < P_0$, V_{lens} is more than V_{other}. In this paper, P_1 is at $P_0 + 78$ Pa when splitting, and P_2 is varied from P_0 to $P_0 + 1995$ Pa by gradually pumping air into the lens channel. Fig. 5(c) shows that the volume of the lens droplet is linearly increased with respect to $P_1 - P_2$ or ΔP_{12} ($P_1 - P_0$ or ΔP_{10} is almost unchanged during splitting). The error bars in Fig. 5(c) reflect the accuracy of controlling the size of the lens droplet; the accuracy is roughly $\pm 8\%$. This inaccuracy could be caused by the compressive nature of air

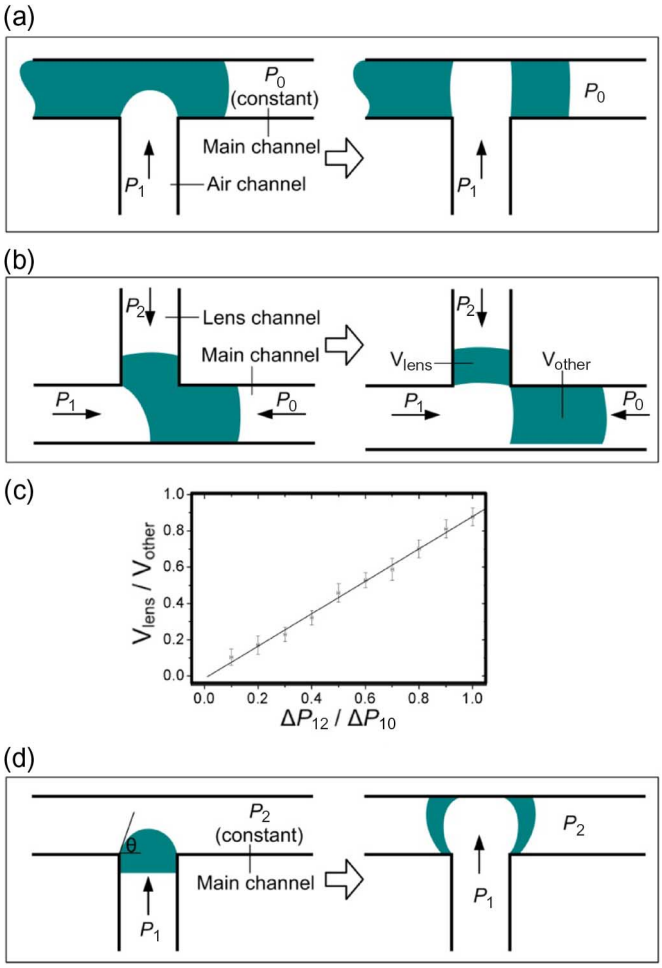

Fig. 5. Pneumatic control of fluids within microchannels. (a) Schematic of cutting a droplet out of a static flow. (b) Schematic of separation of a water droplet using pneumatic pressure. (c) Controlling the size of a lens droplet. Experimental result of the relationship between $V_{\rm lens}/V_{\rm other}$ and $\Delta P_{12}/\Delta P_{10}$, where $V_{\rm lens}$ and ΔP_{12} are the volume of the lens droplet and the pressure difference across it, respectively, and $V_{\rm other}$ and ΔP_{10} are the volume of the droplet remaining in the main channel after separation and the pressure difference across it, respectively. The error bars are the standard deviations of the data points obtained by repeating the experiments for ten times. (d) Schematic of measuring the critical-pressure difference over a liquid microlens.

and the limited accuracy of the pressure sensors used. Although it is true that the air-pressure pneumatic method is not the best solution to accurately control the size of the lens droplet, we believe that there could be much room to improve the accuracy by elaborating the control system (e.g., using feedback circuit between the pressure sensors and the syringe air pumps).

C. Critical Air-Pressure Difference at a Junction

The critical-pressure difference $\Delta P_{\rm CR}$ across a microlens formed at a junction of channels is defined as a minimum pressure drop, above which this droplet tends to be pushed to leave this junction. At a lower pressure drop over the microlens, the liquid–air interface of the microlens, which is pinned at the edges of the junction, appears to be curved while remaining at the junction. As the pressure drop increases, the angle of curvature of the lens droplet [θ in Fig. 5(d)] increases. Increasing θ up to (or even higher than) the value of the contact angle of the liquid ($\theta_{\rm C}$) causes the droplet to break away from the junction. When the liquid–air interface at the edges of the junction is curved, there is a pressure drop across it due to surface free energy. Generally, a pressure drop over a stationary curved fluid interface is expressed with Young–Laplace equation as $\Delta P = \gamma[(1/R_1) + (1/R_2)]$ [43], where ΔP is the pressure drop, γ is the liquid-surface free energy, and R_1 and R_2 are the radii of curvature in directions parallel and vertical, respectively, to the optical axis of the microlens. Due to the surface-chemistry treatment (see Section III-B3), the water–air interface of the droplet is perpendicular to both top and bottom glass slides, and the edges of the water–air interface are pinned at the corners of a T-shaped junction. Thus, the water–air interface is shaped as part of the curved surface of a cylinder, although it is true that there exist slight distortions near the edges. Here, R_2 is infinite, and the equation is simplified to $\Delta P = 2\gamma \sin\theta/d$, where d is the width of the channel. For the other interface of the lens droplet, both R_1 and R_2 are infinite; thus, there is no pressure drop across it. For a stationary microlens, the applied pressure difference and the internal pressure are in equilibrium. Based on the boundary condition for breaking the lens droplet ($\theta = \theta_{\rm C}$), the critical-pressure difference is thus $\Delta P_{\rm CR} = 2\gamma \sin\theta_{\rm C}/d$.

We have measured $\Delta P_{\rm CR}$ of two lens droplets at J3 and J4, respectively. In this paper, P_1 is swept from $P_0 + 15$ Pa to $P_0 + 300$ Pa in steps of 10 Pa by injecting air into conduit AC1 at a rate of 4.7 μL/ min, whereas P_2 is kept constant. At each pressure-difference instance, P_1 holds for 10 s (resident time) to ensure that the lens droplet is stationary. It is found that $\Delta P_{\rm CR}$ for the droplets at J3 and J4 are $\Delta P_{\rm J3} = 215 \pm 5$ Pa and $\Delta P_{\rm J4} = 205 \pm 4.5$ Pa, respectively, which agree well with the theoretical values (219 Pa for J3, and 203 Pa for J4).

V. *In Situ* Formation of Liquid Microlenses

A. Formation of a Single Liquid Microlens

As shown in Fig. 6, to form a single liquid microlens, valve V1 is closed, whereas valve V2 is open; thus, the initial air pressure in the channels is set at P_0. A main water stream is first flowed into the main channel using a syringe fluidic pump through the fluidic inlet at an infusion rate of 0.5 mL/min [Fig. 6(a)]. It is then split into two channels (AC1 and main channel) at junction J1. Subsequently, the fluidic pump stops pumping, whereas the syringe air pump S1 starts injecting an air plug (volume: 16.2 μL; pressure: 1 atm; infusion rate: 0.9 mL/min) into the air conduit AC1 through tubing 1 (inner volume: 676 μL). This dispels the water in AC1 back into the main channel and separates a water droplet from the main water stream [Fig. 6(b)]. Once the injection of the designated air plug is complete, the air pump stops pumping, and the water stream on the left side of J1 is stuck in the main channel. The separated droplet is pushed to move along the main channel under P_1 (P_1 decreases as this droplet advances).

Next, when this separated droplet arrives at junction J2, a small droplet is flowed into the lens channel, whereas the water remaining in the main channel continues to advance in the main channel [Fig. 6(c)]. At the moment that the small droplet is

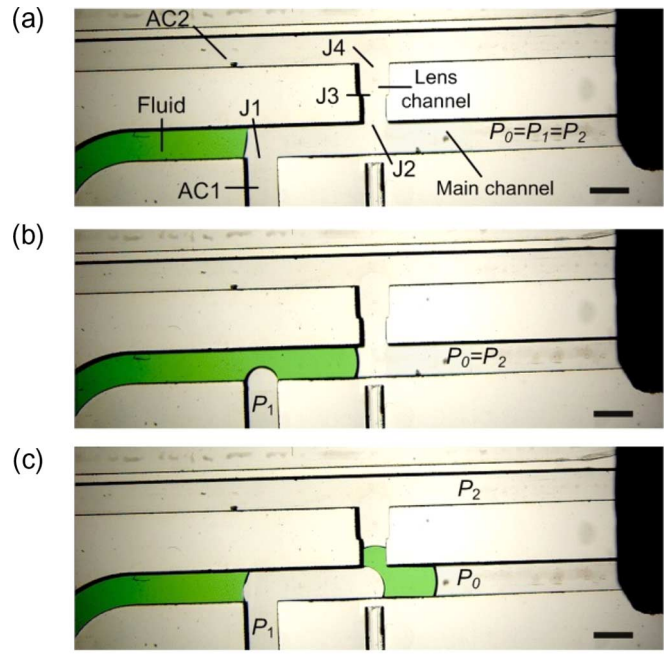

Fig. 6. *In situ* formation process of a liquid microlens within microfluidics. (a) Stream is flowed into the main channel, and syringe air pump S1 starts injection. (b) Water droplet is cut out of the main stream by air pressure P_1 at junction J1. (c) Lens droplet is split into the lens channel at junction J2, and syringe air pump S2 starts injection.

completely separated, a lens droplet is produced [Fig. 6(d)]. To control the volume of the lens droplet, air pressure P_2 is applied to the lens droplet from syringe air pump S2. Here, S2 is programmed to inject an air plug (volume: 10.5 μL; pressure: 1 atm; infusion rate: 0.9 mL/min) into the air conduit AC2 through tubing 2 (inner volume: 585 μL). This causes the lens droplet to be approximately 25% of the whole separated droplet.

Subsequently, this lens droplet moves to junction J3 in the lens channel under both P_1 and P_2, and it stops and remains at J3 where $\Delta P_{12} = P_1 - P_2 = 120$ Pa is programmed to be less than the critical pressure [Fig. 6(e)]. The front liquid–air interface is pinned at the edges of the corner of the junction and curves outward. The other liquid–air interface is found to be a little curved, which could be straight when the smoothness of the sidewalls is improved. Thus, using this *in situ* formation process, the liquid microlens is formed and stably stays at J3.

The status of the microlens can be changed by applying an appropriate ΔP_{12}, which will be described later. In order to change P_1 and P_2 at both sides of the microlens by pumping air into or sucking air out of the corresponding channels, valve V2 is closed (valve V1 is closed at the beginning of the fluid manipulation) when the water remaining in the main channel arrives at V2. The pressure profiles of P_1 and P_2 involved are shown in Fig. 6(f), showing that it only takes approximately 10 s to make the liquid microlens by using the *in situ* formation process.

B. Formation of Multiple Liquid Microlenses

A functional optofluidic system often consists of multiple lenses. By repeating the *in situ* formation process with modified

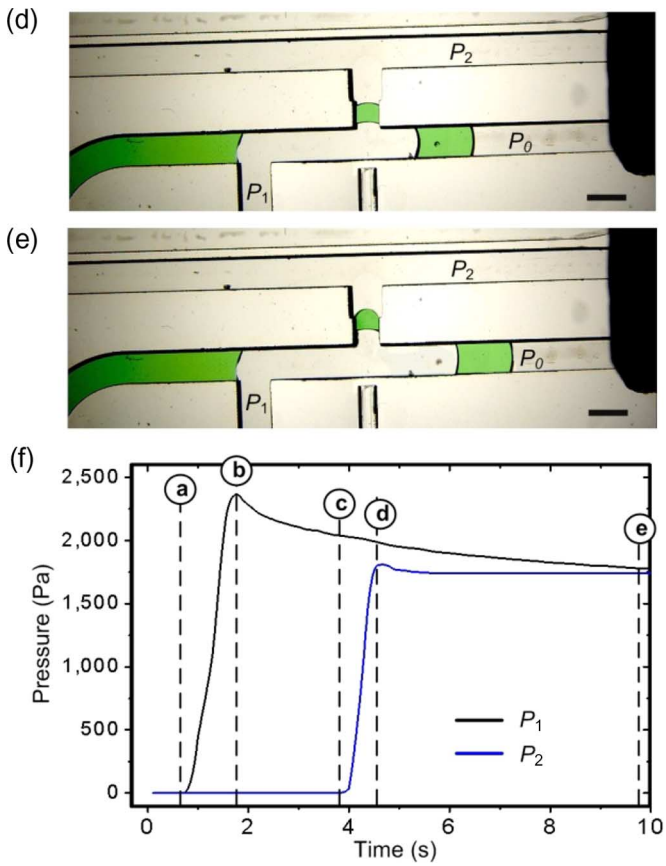

Fig. 6. (*Continued.*) *In situ* formation process of a liquid microlens within microfluidics. (d) Droplet is flowed toward junction J3. (e) Droplet stops at junction J3 and is pinned at the edges of the corners of a small step in the lens channel. Valve V2 is turned off when the droplet remaining in the main channel moves to this valve. P_0 denotes atmospheric pressure. P_1 and P_2 denote the pressures from air channels AC1 and AC2, respectively. (f) Pressure profiles of P_1 and P_2 measured during the *in situ* formation of the microlens depicted in (a)–(e). The y-axis refers to the relative values of P_1 and P_2 above the atmospheric pressure P_0. The characters that are encircled refer to the corresponding steps shown in (a)–(e). Scale bars: 1 mm.

pressure profiles of P_1 and P_2 applied, realizing multiple liquid microlenses is possible. Fig. 7 shows the *in situ* formation of two liquid microlenses in a single lens channel. The first microlens is formed in a way similar to that described in Fig. 6 but at junction J4. Before starting the formation of the second microlens at junction J3, valves V1 and V2 are turned on; thus, both P_1 and P_2 are reset to P_0. Then, V1 is turned off, whereas V2 remains open.

Similar to forming the first microlens, a water droplet is cut out of the main stream at J1 and moves to J2 where a lens droplet for the second microlens is split from the main channel to the lens channel by properly applying P_1 and P_2 [Fig. 7(a) and (b)]. In the experiment shown here, the volume of the second lens droplet is controlled to be approximately 35% of the separated droplet obtained at J1 [Fig. 7(c)]. When this lens droplet flows into the lens channel toward junction J3, the air plug between this droplet and the first microlens is compressed (pressure P_C) and prevents the merging of these two droplets; P_2 ($P_2 > P_C - \Delta P_{J4}$) is applied to prevent the first microlens at J4 from being pushed away (volume of air dispensed from S2: 10.5 μL; infusion rate: 0.9 mL/min) [Fig. 7(d)]. As the rest

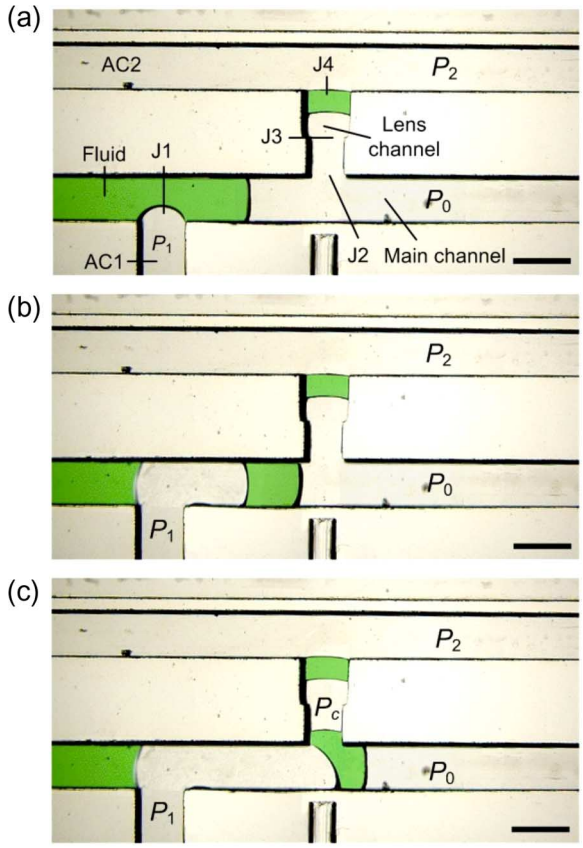

Fig. 7. *In situ* formation of two liquid microlenses in a single channel. (a) Liquid microlens is first formed at junction J4 by repeating the process shown in Fig. 6(a)–(e). A main stream for the second lens stops flowing when it passes through junction J1, and syringe air pump S1 starts injection. (b) Segment of water for the second microlens is cut out of this water stream. (c) Water droplet starts to split into two parts at junction J2, and syringe air pump S2 starts injection.

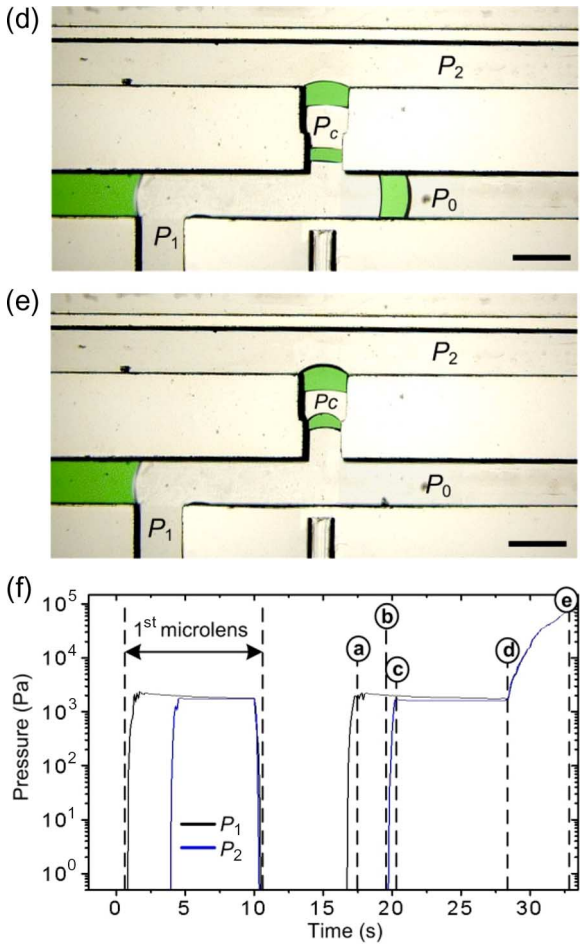

Fig. 7. (*Continued.*) *In situ* formation of two liquid microlenses in a single channel. (d) Lens droplet is flowed into the lens channel. (e) Lens droplet is moved to and pinned at junction J3 by adjusting air pressures P_1 and P_2. Valve V1 is turned off when the droplet remaining in the main channel moves to this valve. Then, S1 and S2 simultaneously inject two air plugs into air channels AC1 and AC2, respectively. Scale bars: 1 mm. (f) Pressure profiles of P_1 and P_2 measured during the *in situ* formation of these two microlenses. The y-axis (logarithmic) refers to the relative values of P_1 and P_2 over atmospheric pressure P_0. The characters that are encircled refer to the corresponding steps in (a)–(e). Scale bars: 1 mm.

of the water remaining in the main channel reaches valve V2, V2 is turned off [Fig. 7(e)].

In order to move the second lens to and stop at J3, P_1 and P_2 are adjusted to be $P_1 < P_C + \Delta P_{J3}$ and $P_2 > P_C - \Delta P_{J4}$ by dispensing air plugs of 458 μL (infusion rate of S1: 5.5 mL/min) and 417 μL (infusion rate of S2: 5.0 mL/min) into AC1 and AC2, respectively. Therefore, both liquid microlenses are formed and can stably stay at their own junctions within the lens channel. The whole process is complete within 30 s. The pressure profiles of P_1 and P_2 involved in this case are shown in Fig. 7(f). It is also interesting to point out that, by using a series of independent microfluidic channel networks, a 2-D microlens array could be formed with different numbers of multiple lens elements in each lens channel.

VI. Reconfiguration of Liquid Microlenses

By varying the air-pressure difference across the microlens with proper pneumatic control, the microlens can be reconfigured in terms of its location and presence in the microchannel network and in terms of its focal length. We have demonstrated that the liquid microlens can be tuned in focal length and can be repositioned, removed, and reformed at predetermined locations within microchannels. Here, both V1 and V2 are turned off all the time unless the air pressures need to be reset to atmospheric pressure for reforming a microlens or the lens droplets need to be removed to the waste reservoirs. The air pressures inside the channels are controlled by using the syringe air pumps. The value of P_1 and P_2 can be predetermined using the ideal gas law expressed by $P_{\rm i}V_{\rm i}/T_{\rm i} = P_{\rm f}V_{\rm f}/T_{\rm f}$, where the subscripts i and f refer to the initial and final states of the gas system, respectively.

A. Repositioning

To reposition a microlens from one junction to another, we increase ΔP_{12} across the microlens to be more than the critical pressure at the initial junction and then adjust ΔP_{12} to be less than the critical pressure at the new junction. As shown in Fig. 8(a)–(c), the microlens is first pinned at junction J3, and P_1 and P_2 are $P_0 + 1768$ Pa and $P_0 + 1755$ Pa, respectively. To force the microlens to leave J3, ΔP_{12} is increased to approximately 225.5 Pa by retracting 2.5 μL of air plug

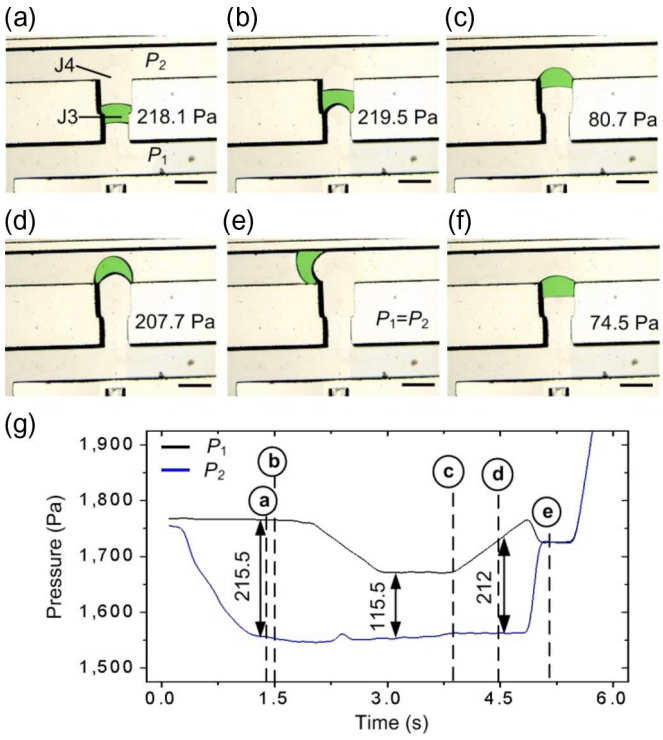

Fig. 8. Repositioning, removing, and reforming a liquid microlens. (a)–(c) Microlens is repositioned from junction J3 to junction J4. (d) and (e) Microlens is removed from J4. (f) New lens is formed at J4 by repeating the *in situ* formation process. The data in each snapshot show the pressure difference ($\Delta P_{12} = P_1 - P_2$) across the microlens. (g) Pressure profiles involved in (a)–(e). The y-axis refers to the relative values of P_1 and P_2 over atmospheric pressure P_0. The characters that are encircled refer to the corresponding steps in (a)–(e). Scale bars: 1 mm.

from syringe air pump S2 at a rate of 0.15 mL/min ($\Delta P_{\mathrm{J3}} = 215 \pm 5$ Pa). After the droplet gets away from J3 completely, 1.5 μL of air plug is immediately retracted from S1 at a rate of 0.35 mL/min to decrease P_1, which renders a ΔP_{12} at J4 less than $\Delta P_{\mathrm{J4}} = 205 \pm 4.5$ Pa. Consequently, the microlens is stopped and pinned at J4.

B. Removal and Reformation

To remove the microlens at junction J4, ΔP_{12} needs to be increased above ΔP_{J4}. We inject 2.7 μL of air plug from syringe air pump S1 at a rate of 0.2 mL/min, and the lens droplet is pushed away from J4. Then, valve V1 is turned on. Finally, both P_1 and P_2 are increased to push the lens droplet into the waste reservoir through V1. Fig. 8(d) and (e) shows how the microlens breaks the geometrical obstruction at J4 and flows into the waste reservoir. The pressure profiles of P_1 and P_2 involved in repositioning and removal of the microlens are shown in Fig. 8(g). After the pathway of AC2 is cleared up by air, we reform a new liquid microlens at J4 [Fig. 8(f)] in place of its predecessor by repeating the *in situ* formation process shown in Fig. 6.

C. Tuning of a Single Liquid Microlens

By varying the pressure difference across a lens pinned at a junction, while keeping it less than the critical value, the shape

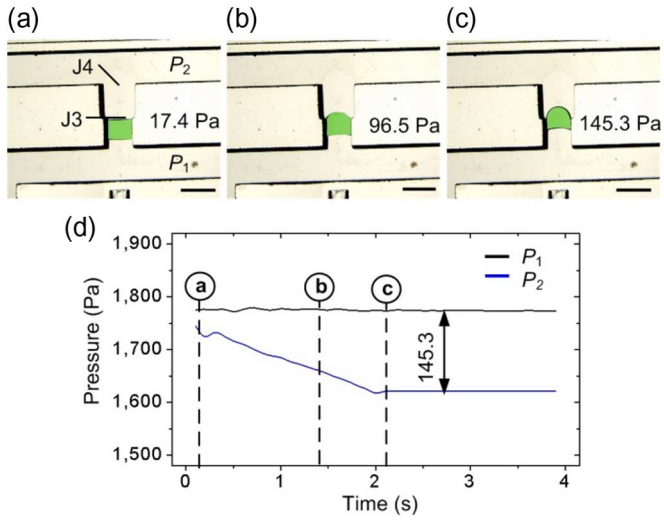

Fig. 9. Tuning a liquid microlens. (a)–(c) Microlens is tuned at J3. The data in each snapshot show the pressure difference ($\Delta P_{12} = P_1 - P_2$) across the microlens. (d) Pressure profiles of P1 and P2 involved in tuning the lens. The y-axis refers to the relative values of P_1 and P_2 over atmospheric pressure P_0. The characters that are encircled refer to the corresponding steps in (a)–(c). Scale bars: 1 mm.

of the microlens can be adjusted; for each pressure difference, the microlens is able to maintain a stable state. As shown in Fig. 9(a)–(c), initially, the microlens is pinned at J3, and P_1 and P_2 are $P_0 + 1775$ Pa and $P_0 + 1744.8$ Pa, respectively. Then, P_2 is gradually decreased to $P_0 + 1620$ Pa by retracting an air plug (volume: 1.6 μL; rate: 48 $\mu\mathrm{L}/\mathrm{min}$) out of AC2, whereas P_1 is held constant. The microlens becomes more curved, thus having a decreased focal length. The new shape of the microlens is stable as long as the pressure difference is constant [Fig. 9(d)]. The repositioned microlens can be tuned as well while being stably pinned at the corners of J4.

D. Tuning of a Two-Microlens System

Both microlenses in the two-lens system shown in Fig. 7 can be tuned in shape. For example, decreasing P_2 renders a more convex microlens at J4 [Fig. 10(a)]; this, however, also leads to a slight change in the shape of the microlens at J3 due to the volume change of the air plug between these two microlenses. By subsequently adjusting P_1, the microlens at junction J3 shown in Fig. 10(b) can be adjusted to be the same as that in Fig. 10(a). Therefore, the focal length of each microlens in a multiple-microlens system can be tuned, whereas the other microlenses are able to recover their original focal lengths. This is conducive to the design of optical systems within microfluidics, giving great flexibility in the configuration of compound microlenses.

VII. Characterization

A. Tuning Focused Point of Light

To examine the shift of the focused point of the light passing through a liquid microlens, we integrate a detection channel, an optical fiber (outer diameter: 470 μm; core diameter: 400 μm, 0.22 NA; Edmund Optics, Barrington, NJ), and an

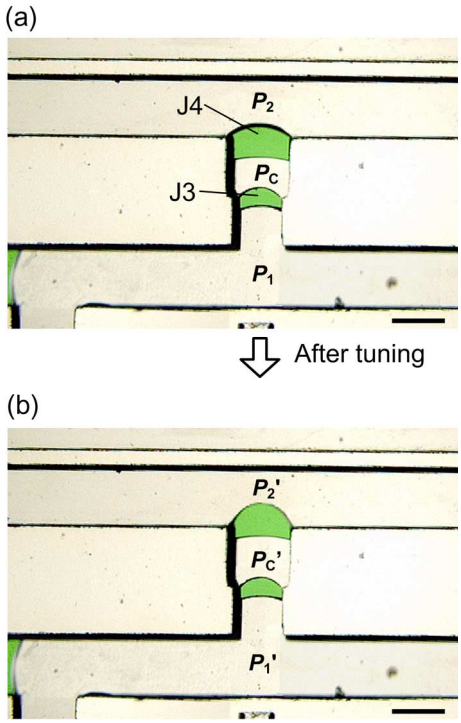

Fig. 10. Tuning a liquid microlens in a two-lens combination. Scale bars: 1 mm.

in situ-formed microlens on the same substrate. An incident light transmits along the optical fiber that is previously integrated into the poly(IBA) construction material. The detection channel is separately fabricated adjacent to the microlens.

As shown in Fig. 11, three laminar streams flow in a detection channel (1.0 mm wide) close to air conduit AC2. Each stream is controlled by a syringe fluid pump. The stream ($\sim$50 μm wide) between two water streams contains fluorescein (fluorescein sodium salt; 460-nm excitation; 515-nm emission; 100-μM concentration; Sigma–Aldrich, Inc., St. Louis, MO). Fluorescent light can emit from this stream under incident excitation light through the microlens being tested. Here, the incident light (light source: a light-emitting diode located 55 mm away from the detection channel; peak wavelength: 470 nm; working voltage: 3.5 V; Kingbright Corporation, City of Industry, CA) passes an optical bandpass filter (central wavelength: 467 nm; full-width at half-maximum: 10 nm; Edmund Optics, Barrington, NJ) and couples into a collimator (VIS 0.25NA FC Focuser, Edmund Optics, Barrington, NJ) and an optical fiber. A fluorescence stereoscope [Olympus (model SZX12), Melville, NY] coupling to a charge-coupled-device (CCD) camera [Leica Microsystems (model DFC300 FX), Allendale, NJ] is used to record images. By adjusting the pressure difference across the microlens, the focused point of the excitation light moves across the width of the detection channel. When the focused point is on the stream containing the fluorescein, the fluorescent emission becomes strongest as illustrated. The distance between the central line of this stream and the lower wall of air conduit AC2 [see d in Fig. 11(a)] is then recorded. Fig. 12 (y-axis on the left side) shows the measured shift of the focused point (i.e., a change in d) by varying the air-pressure difference across the microlens. The error ranges on the y-axis

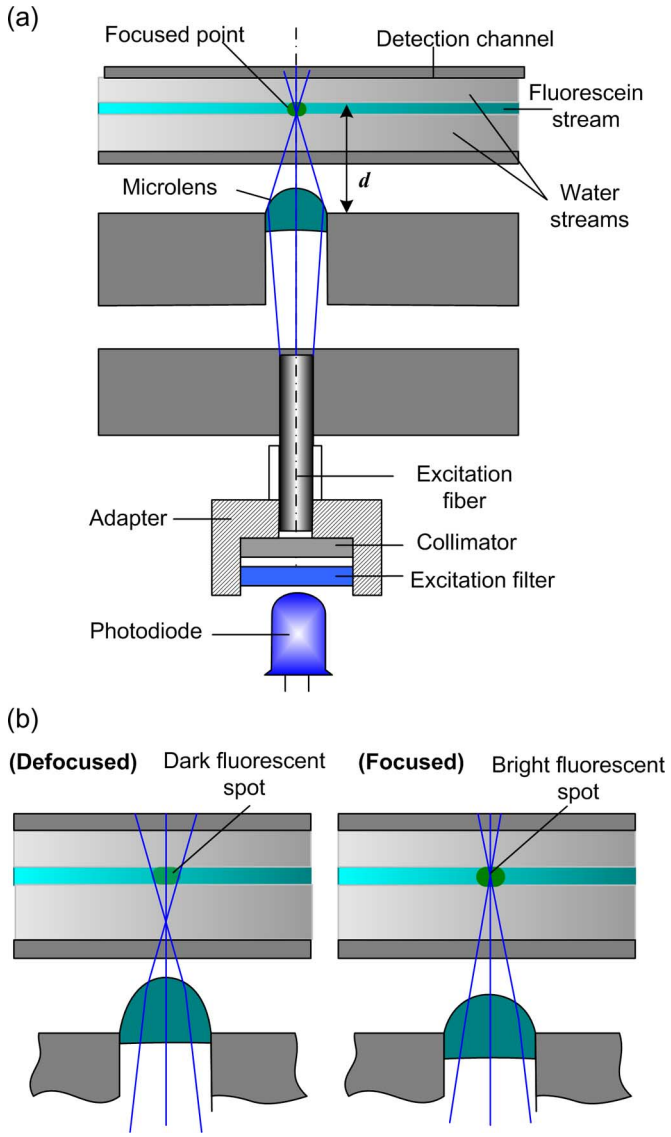

Fig. 11. (a) Schematic of a measurement setup to examine the shift of the focused point of the light passing through a liquid microlens. (b) Fluorescent spots when excitation light is focused onto and defocused from a stream containing fluorescein.

on the right are $\pm$0.14, $\pm$0.1, $\pm$0.05, and $\pm$0.02 mm at 105, 148, 177, and 202 Pa, respectively. At each pressure difference, we repeat the measurements ten times by generating the laminar streams and adjusting their position to allow the excitation light to be focused on the middle stream containing fluorescent dye. Then, the mean position of the middle stream and the standard-deviation error bars are calculated. In this paper, no significant hysteresis in the position of the focused point of light is found by increasing and decreasing pressure difference.

The focal lengths of the microlens at varying pressure differences are also calculated by measuring the curvatures of the liquid–air interfaces. Since the water–air interfaces appear perpendicular to both top and bottom chemically treated substrates, the curvature measurement may be a reliable way to estimate the focal length. The shapes of these liquid–air interfaces are taken by a CCD camera [Leica Microsystems (model DFC300 FX), Allendale, NJ] connected to a stereoscope [Olympus (model SZX12), Melville, NY]. The focal length f

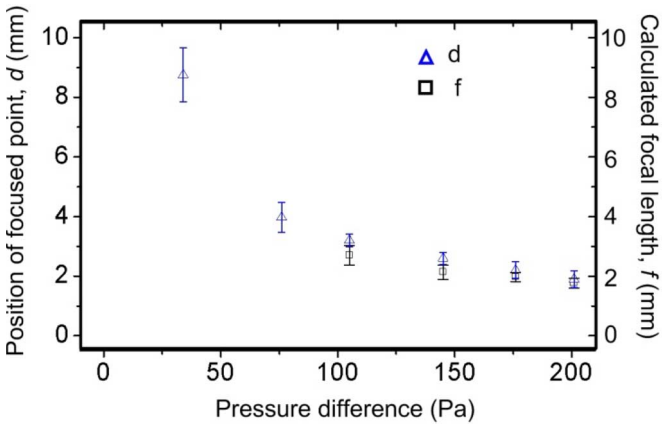

Fig. 12. Shift of the focused point of the light passing through a liquid microlens [d (y-axis on the left side) is the distance between the central line of the fluorescein stream and the lower wall of air conduit AC2; see d in Fig. 11(a)] and the calculated focal length of a microlens (y-axis on the right side, f) at various pressure differences across the lens.

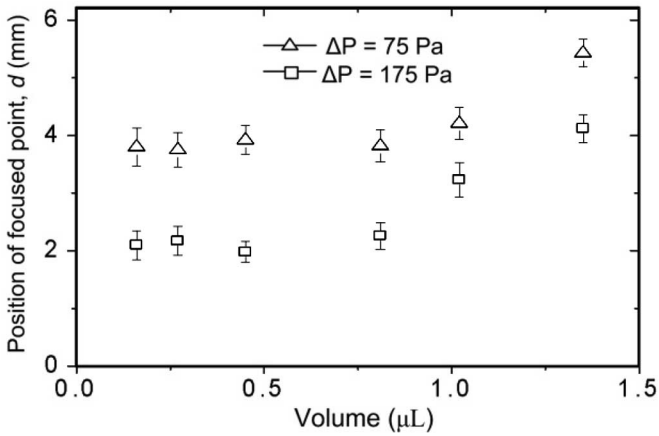

Fig. 13. Dependence of the shift of the focused point of the light passing through a liquid microlens [d is the distance between the central line of the fluorescein stream and the lower wall of air conduit AC2; see d in Fig. 11(a)] on the volume of the lens droplet. For each lens droplet, d is measured at two pressure differences across the lens (ΔP), which are 75 and 175 Pa, respectively.

is estimated by $f = \Delta n(1/r_1 - 1/r_2)$, where $\Delta n = n_1 - n_2$ is the absolute difference in refractive indices between water ($n_1 = 1.33$) and air ($n_2 = 1.0$), and r_1 and r_2 are the radii of curvature of the two air–liquid interfaces of the microlens. To obtain r_1 and r_2, the optical images of the microlens at varying pressure differences are analyzed using the image analysis software for the goniometer (OCA 5, DataPhysics Instruments GmbH, Filderstadt, Germany). Fig. 12 (y-axis on the right side) shows that the calculated focal-length results are consistent. It also shows that the focal length can be dynamically controlled through tuning the pressures, varying from 1.5 to 8.9 mm over ΔP that is from 30 to 201 Pa. As ΔP approaches zero, f approaches infinity.

B. Position of Focused Point of Light Versus Lens-Droplet Size

Fig. 13 shows the relationship between the lens-droplet size and the focused point of the excitation light. The lens channel used here is 0.75 mm wide, 5 mm long, and 0.45 mm deep. Six lens droplets with volumes of 0.16, 0.27, 0.45, 0.81, 1.02, and 1.35 μL, respectively, are generated at junction J4. For each lens droplet, we measure the corresponding d at two pressure differences across the microlens, which are 75 and 175 Pa, respectively. For a given pressure difference, d is almost independent of the volume of the lens droplet until 0.81 μL and then slightly increases with increasing volumes. The constant focal length at the small volumes is reasonable since the thickness of the thin lens is negligible compared to the focal length of the lens. As the volume of the lens droplet increases, the microlens converts from a thin lens to a thick one, thus causing its focal length to increase [46]. Here, the position of the focused point of the excitation light is measured by the same method as in Section VII-A earlier.

VIII. Conclusion

In conclusion, we have described the design, formation, and characterization of liquid microlenses that are *in situ*-formed via pinned cylindrical liquid–air interfaces and have optical axes parallel to the substrate used. The microlenses not only have wide tuning range in the focal lengths (a few hundreds of micrometers to ∞) but also can be repositioned, removed, and reformed at predetermined locations of T-shaped junctions within microchannels on demand under pneumatic controls. This would be relatively difficult to realize by other methods. Therefore, users have more flexibility in designing microoptics within microfluidics.

Since the optical axes of these microlenses are parallel to the glass slides used, light can transmit within highly transparent channel materials, such as PDMS and silica glass, and can directly couple into other microfabricated optical components that usually have planar structure (e.g., waveguide, optical fiber, and reflective mirror). In comparison, microfabricated fixed and tunable lenses usually have their optical axes perpendicular to the substrates, and a common integration approach is to fabricate the microlenses on top of the corresponding microfluidic devices. Therefore, the optical axis of the microlens parallel to the substrate used allows for the use of a single-layer infrastructure to realize complicated on-chip optics that would otherwise involve multiple layers and different materials. Also, since these microlenses are formed within the microfluidic channels, it is possible to self-align the microlenses to a specific area in the channel. Conventionally, the optical alignment is manually carried out after each functional component is fabricated on different layers, which often causes misalignment between these optical components. With this lens technology, the alignment of the microlens with a designated area in a microchannel can be predetermined when the user designs a single photomask for the entire microchannel network, eliminating additional optical alignment and assembling steps. Note the ability to realize multiple *in situ*-formed microlenses; it allows for compound configurations of the microlenses for more complex functionality. Although the fluid manipulation in this paper is implemented pneumatically, other fluid-control methods such as electrowetting [47] and photothermal control [48] could be applied to realize precise fluid manipulation. In addition, new functions can be explored—for example, individual control of

multiple microlenses in microchannels is possible by electrically addressing one lens droplet and modifying the surface energies associated with the liquid–air and solid–liquid interactions. Also, other chemical surface treatments (e.g., photocleavable self-assembled monolayer technology [49]) may be used to pattern surface energies to form hydrophobic–hydrophilic contact lines, thus replacing the physical edges defined by the geometry of the junctions. We believe that the technology described here provides great flexibility in the design and formation of microlenses within microfluidics and may find many applications, such as sensing and medical diagnostics, where lab-on-a-chip technologies and microoptics are important. For instance, it could be implemented in bioanalytical devices that integrate optical elements into microfluidic devices in ways that increase reconfigurability, portability, and sensitivity.

ACKNOWLEDGMENT

The authors would like to thank D. J. Beebe (University of Wisconsin, Madison) and his research group for the fruitful discussions and access to their facilities. The authors would also like to thank S. S. Sridharamurthy and X. Zeng for the technical assistance. H. Jiang would also like to thank 3M (St. Paul, MN) for his Non-Tenured Faculty Award.

REFERENCES

[1] K. Carlson, M. Chidley, K. B. Sung, M. I. Descour, A. Gillenwater, M. Follen, and R. Richards-Kortum, "*In vivo* fiber-optic confocal reflectance microscope with an injection-molded plastic miniature objective lens," *Appl. Opt.*, vol. 44, no. 10, pp. 1792–1797, 2005.

[2] G. Tearney, M. E. Brezinski, B. E. Bouma, S. A. Boppart, C. Pitris, J. F. Southern, and J. G. Fujimoto, "In vivo endoscopic optical biopsy with optical coherence tomography," *Science*, vol. 276, no. 5321, pp. 2037–2039, Jun. 1997.

[3] J. Rosen and D. Abookasis, "Seeing through biological tissues using the fly eye principle," *Opt. Express*, vol. 11, no. 26, pp. 3605–3611, Dec. 2003.

[4] C. A. Edwards, H. M. Presby, and C. Dragone, "Ideal microlenses for laser to fiber coupling," *J. Lightw. Technol.*, vol. 11, no. 2, pp. 252–257, Feb. 1993.

[5] J. Lim, G. B. Jeong, S. M. Kim, J. Han, J. M. Yoo, N. C. Park, and S. Kang, "Design and fabrication of a diffractive optical element for the objective lens of a small form factor optical data storage device," *J. Micromech. Microeng.*, vol. 16, no. 1, pp. 77–82, Jan. 2006.

[6] J. Aizenberg, A. Tkachenko, S. Weiner, L. Addadi, and G. Hendler, "Calcitic microlenses as part of the photoreceptor system in brittlestars," *Nature*, vol. 412, no. 6849, pp. 819–822, Aug. 2001.

[7] K. H. Jeong, J. Kim, and L. P. Lee, "Biologically inspired artificial compound eyes," *Science*, vol. 312, no. 5773, pp. 557–561, Apr. 2006.

[8] J. Kim, N. Singh, and L. A. Lyon, "Label-free biosensing with hydrogel microlenses," *Angew. Chem. Int. Ed.*, vol. 45, no. 9, pp. 1446–1449, 2006.

[9] M. L. Chabinyc, D. T. Chiu, J. C. McDonald, A. D. Stroock, J. F. Christian, A. M. Karger, and G. M. Whitesides, "An integrated fluorescence detection system in poly(dimethylsiloxane) for microfluidic applications," *Anal. Chem.*, vol. 73, no. 18, pp. 4491–4498, Sep. 2001.

[10] T. Kamei, B. M. Paegel, J. R. Scherer, A. M. Skelley, R. A. Street, and R. A. Mathies, "Fusion of a-Si:H sensor technology with microfluidic bioanalytical devices," *J. Non-Cryst. Solids*, vol. 338, pp. 715–719, Jun. 2004.

[11] A. Jain and H. Xie, "Microendoscopic confocal imaging probe based on an LVD microlens scanner," *IEEE J. Sel. Topics Quantum Electron.*, vol. 13, no. 2, pp. 228–234, Mar./Apr. 2007.

[12] J. C. Roulet, R. Volkel, H. P. Herzig, E. Verpoorte, N. F. de Rooij, and R. Dandliker, "Microlens systems for fluorescence detection in chemical microsystems," *Opt. Eng.*, vol. 40, no. 5, pp. 814–821, May 2001.

[13] S. Camou, H. Fujita, and T. Fujii, "PDMS 2D optical lens integrated with microfluidic channels: Principle and characterization," *Lab Chip*, vol. 3, pp. 40–45, 2003.

[14] J. Hubner, K. B. Mogensen, A. M. Jorgensen, P. Friis, P. Telleman, and J. P. Kutter, "Integrated optical measurement system for fluorescence spectroscopy in microfluidic channels," *Rev. Sci. Instrum.*, vol. 72, no. 1, pp. 229–233, 2001.

[15] J. R. Wendt, M. E. Warren, W. C. Sweatt, C. G. Bailey, C. M. Matzke, D. W. Arnold, A. A. Allerman, T. R. Carter, R. E. Asbill, and S. Samora, "Fabrication of high performance microlenses for an integrated capillary channel electrochromatograph with fluorescence detection," *J. Vac. Sci. Technol. B, Microelectron. Process. Phenom.*, vol. 17, no. 6, pp. 3252–3255, Nov. 1999.

[16] J. M. Jang, H. J. Shin, S. W. Hwang, and E. G. Yang, "Miniaturized fluorescence detection system to remove background noise of the incident light using micro mirror and lens," *Sens. Actuators B, Chem.*, vol. 108, no. 1/2, pp. 993–1000, Jul. 2005.

[17] J. Seo and L. P. Lee, "Disposable integrated microfluidics with self-aligned planar microlenses," *Sens. Actuators B, Chem.*, vol. 99, no. 2/3, pp. 615–622, May 2004.

[18] S. Haselbeck, H. Schreiber, J. Schwider, and N. Streibl, "Microlenses fabricated by melting a photoresist on a base layer," *Opt. Eng.*, vol. 32, no. 6, pp. 1322–1324, Jun. 1993.

[19] H. H. Yang, C. K. Chao, M. K. Wei, and C. P. Lin, "High fill-factor microlens array mold insert fabrication using a thermal reflow process," *J. Micromech. Microeng.*, vol. 14, no. 8, pp. 1197–1204, Aug. 2004.

[20] P. Savander, "Microlens arrays etched into glass and silicon," *Opt. Lasers Eng.*, vol. 20, no. 2, pp. 97–107, 1994.

[21] K. P. Larsen, J. T. Ravnkilde, and O. Hansen, "Investigations of the isotropic etch of an ICP source for silicon microlens mold fabrication," *J. Micromech. Microeng.*, vol. 15, no. 4, pp. 873–882, Apr. 2005.

[22] S. Biehl, R. Danzebrink, P. Oliveira, and M. A. Aegerter, "Refractive microlens fabrication by ink-jet process," *J. Sol-Gel Sci. Technol.*, vol. 13, no. 1–3, pp. 177–182, Jan. 1998.

[23] H. Choo and R. S. Muller, "Addressable microlens array to improve dynamic range of Shack–Hartmann sensors," *J. Microelectromech. Syst.*, vol. 15, no. 6, pp. 1555–1567, Dec. 2006.

[24] P. Ruther, B. Gerlach, J. Göttert, M. Ilie, J. Mohr, A. Müller, and C. Oßmann, "Fabrication and characterization of microlenses realized by a modified LIGA process," *Pure Appl. Opt.*, vol. 6, no. 6, pp. 643–653, Nov. 1997.

[25] S. K. Lee, K. C. Lee, and S. S. Lee, "A simple method for microlens fabrication by the modified LIGA process," *J. Micromech. Microeng.*, vol. 12, no. 3, pp. 334–340, May 2002.

[26] R. R. A. Syms, "Refractive collimating microlens arrays by surface tension self-assembly," *IEEE Photon. Technol. Lett.*, vol. 12, no. 11, pp. 1507–1509, Nov. 2000.

[27] O. J. Cayre and V. M. Paunov, "Fabrication of microlens arrays by gel trapping of self-assembled particle monolayers at the decane–water interface," *J. Mater. Chem.*, vol. 14, no. 22, pp. 3300–3302, 2004.

[28] S. Yang, T. N. Krupenkin, P. Mach, and E. A. Chandross, "Fabrication of tunable and latchable liquid microlens with photopolymerizable components," *Adv. Mater*, vol. 15, no. 11, pp. 940–943, 2003.

[29] H. Jiang and L. Dong, "Smart lenses," *Physics World*, vol. 19, no. 11, pp. 29–31, 2006.

[30] V. V. Presnyakov, K. E. Asatryan, T. V. Galstian, and A. Tork, "Polymer-stabilized liquid crystal for tunable microlens applications," *Opt. Experss*, vol. 10, no. 17, pp. 865–870, Aug. 2002.

[31] H. W. Ren, Y. H. Fan, S. Gauza, and S. T. Wu, "Tunable microlens arrays using polymer network liquid crystal," *Opt. Commun.*, vol. 230, no. 4–6, pp. 267–271, Feb. 2004.

[32] S. Kuiper and B. H. W. Hendriks, "Variable-focus liquid lens for miniature cameras," *Appl. Phys. Lett.*, vol. 85, no. 7, pp. 1128–1130, Aug. 2004.

[33] T. Krupenkin, S. Yang, and P. Mach, "Tunable liquid microlens," *Appl. Phys. Lett.*, vol. 82, no. 3, pp. 316–318, Jan. 2003.

[34] C. A. Lopez, C. C. Lee, and A. H. Hirsa, "Electrochemically activated adaptive liquid lens," *Appl. Phys. Lett.*, vol. 87, no. 13, p. 134 102, Sep. 2005.

[35] D. Y. Zhang, V. Lien, Y. Berdichevsky, J. Choi, and Y. H. Lo, "Fluidic adaptive lens with high focal length tenability," *Appl. Phys. Lett.*, vol. 82, no. 19, pp. 3171–3172, May 2003.

[36] N. Chronis, G. L. Liu, K. Jeong, and L. P. Lee, "Tunable liquid-filled microlens array integrated with microfluidic network," *Opt. Express*, vol. 11, no. 19, pp. 2370–2378, 2003.

[37] L. Dong, A. K. Agarwal, D. J. Beebe, and H. Jiang, "Adaptive liquid microlenses activated by stimuli-responsive hydrogels," *Nature*, vol. 442, no. 7102, pp. 551–554, Aug. 2006.

[38] L. Dong, A. K. Agarwal, D. J. Beebe, and H. Jiang, "Variable-focus liquid microlenses and microlens arrays actuated by thermoresponsive hydrogels," *Adv. Mater.*, vol. 19, no. 3, pp. 401–405, Feb. 2007.

[39] L. Dong and H. Jiang, "pH-adaptive microlenses using pinned liquid–liquid interfaces actuated by pH-responsive hydrogel," *Appl. Phys. Lett.*, vol. 89, no. 21, art. no. 211120, Nov. 2006.
[40] J. Kim, M. J. Serpe, and L. A. Lyon, "Hydrogel microparticles as dynamically tunable microlenses," *J. Amer. Chem. Soc.*, vol. 126, no. 31, pp. 9512–9513, 2004.
[41] L. Dong and H. Jiang, "Liquid microlenses capable of both *in situ* integration within microfluidics and real-time tuning," in *Proc. 20th IEEE Int. Conf. MEMS*, Kobe, Japan, Jan. 2007, pp. 151–154.
[42] L. Dong and H. Jiang, "Tunable and movable liquid microlens *in situ* fabricated within microfluidic channels," *Appl. Phys. Lett.*, vol. 91, no. 4, art. no. 041109, Jul. 2007.
[43] J. Atencia and D. J. Beebe, "Controlled microfluidic interfaces," *Nature*, vol. 437, no. 7059, pp. 648–655, Sep. 2005.
[44] D. J. Beebe, J. Moore, Q. Yu, R. H. Liu, M. L. Kraft, B.-H. Jo, and C. Devadoss, "Microfluidic tectonics: A comprehensive construction platform for microfluidic systems," *Proc. Nat. Acad. Sci. U.S.A.*, vol. 97, no. 25, pp. 13 488–13 493, Dec. 2000.
[45] A. K. Agarwal, S. S. Sridharamurthy, D. J. Beebe, and H. Jiang, "Programmable autonomous micromixers and micropumps," *J. Microelectromech. Syst.*, vol. 14, no. 6, pp. 1409–1421, Dec. 2005.
[46] J. R. Meyer-Arendt, *Introduction to Classical and Modern Optics*. Englewood Cliffs, NJ: Prentice-Hall, 1984.
[47] F. Mugele and J. C. Baret, "Electrowetting: From basics to applications," *J. Phys.: Condens. Matter*, vol. 17, no. 28, pp. R705–R774, Jul. 2005.
[48] G. L. Liu, J. Kim, Y. Lu, and L. P. Lee, "Optofluidic control using photothermal nanoparticles," *Nat. Mater.*, vol. 5, no. 1, pp. 27–32, Jan. 2006.
[49] B. Zhao, J. S. Moore, and D. J. Beebe, "Surface-directed liquid flow inside microchannels," *Science*, vol. 291, no. 5506, pp. 1023–1026, Feb. 2001.

Liang Dong (S'03–M'04) received the B.S. degree in precision instrumentation from Xidian University, Xi'an, China, in 1999, and the Ph.D. degree in electrical engineering from Tsinghua University, Beijing, China, in 2004.

He is currently an Assistant Professor with the Department of Electrical and Computer Engineering, Iowa State University, Ames. From 2004 to 2007, he was a Postdoctoral Researcher with the Department of Electrical and Computer Engineering, University of Wisconsin, Madison. His research interests include MEMS/NEMS, bio-MEMS, biosensors, microfluidics, lab-on-a-chip, smart materials, and biomimetics and their applications in biomedical engineering and health care.

Dr. Dong was the recipient of the National Outstanding Doctoral Dissertation Award of China in 2007.

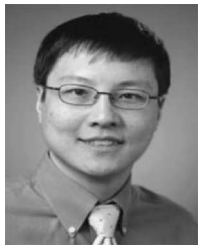

Hongrui Jiang (S'98–M'02) received the B.S. degree in physics from Peking University, Beijing, China, and the M.S. and Ph.D. degrees in electrical engineering from Cornell University, Ithaca, NY, in 1999 and 2001, respectively.

He is currently an Assistant Professor with the Department of Electrical and Computer Engineering, a Faculty Affiliate with the Department of Biomedical Engineering, and a Faculty Member with the Materials Science Program, University of Wisconsin (UW), Madison. Before he joined the faculty at UW—Madison in 2002, he was a Postdoctoral Researcher with the Berkeley Sensor and Actuator Center, University of California—Berkeley, Berkeley, from 2001 to 2002. His research interests are in microfabrication technology, biological and chemical microsensors, microactuators, optical MEMS, smart materials and micro-/nanostructures, and lab-on-a-chip.